

Evidence of Magnetically Driven Structural Phase Transition in Parent Compounds $R\text{FeAsO}$ ($R = \text{La, Sm, Gd, Tb}$): study of low-temperature X-ray diffraction

Yongkang Luo¹, Qian Tao¹, Yuke Li¹, Xiao Lin¹, Linjun Li¹, Guanghan Cao¹, Zhu-an Xu^{1*}, Yun Xue², Hiroshi Kaneko², Andrey V. Savinkov², Haruhiko Suzuki², Chen Fang³, and Jiangping Hu³

¹Department of Physics, Zhejiang University, Hangzhou 310027, China

²Department of Physics, Kanazawa University, Kakuma-machi, Kanazawa 920-1192, Japan

³Department of Physics, Purdue University, West Lafayette, Indiana 47907, USA

(Dated: February 4, 2022)

We report measurements of structural phase transition of four parent compounds $R\text{FeAsO}$ ($R = \text{La, Sm, Gd, and Tb}$) by means of low-temperature X-ray diffraction (XRD). Magnetic transition temperatures associated with Fe ions (T_{N1}) are also determined from the temperature dependence of resistivity. As R is changed from La, through Sm and Gd, to Tb, both the c -axis and a -axis lattice constants decrease significantly. Meanwhile both the structural phase transition temperature (T_S) and T_{N1} decrease monotonously. It is also found that the temperature gap between T_S and T_{N1} becomes smaller when the distance between FeAs layer becomes shorter. This result is consistent with magnetically driven structural phase transition and suggests that the dimensionality have an important effect on the AFM ordering.

PACS numbers: 78.70.Ck; 74.70.Dd; 74.62.Bf; 74.25.Ha

I. INTRODUCTION

The recent discovery of superconductivity in layered pnictide-oxide quaternary compounds $ROTmPn$ ($R = \text{lanthanides, } Tm = \text{Fe, Ni, } Pn = \text{P, As}$) has sparked enormous interest in this class of materials^{1,2,3,4,5,6,7,8}. Besides this 1111-type layered compounds, superconductivity was subsequently discovered in other iron-based layered compounds with similar FeAs(Se) layers, i.e., 122 systems⁹, 111 systems¹⁰, and 11 systems¹¹. In all the FeAs-based parent compounds, there is a structural phase transition in the temperature range 100-200 K, and a stripe-type antiferromagnetic (AFM) ordering associated with Fe ions accompanying the structural transition^{12,13,14}. Various chemical doping approaches can suppress the structural transition and AFM order, and high- T_c superconductivity consequently appears. Meanwhile, low- T_c superconductivity has been observed in undoped FeP-based¹ and NiAs(P)-based^{8,15} compounds with similar layered structure, but there is neither structural transition nor AFM ordering associated with Fe(Ni) ions in these compounds. This result implies that there is a relationship between structural transition/AFM ordering and high- T_c superconductivity. Theoretically, the origin of the AFM order is still controversial. There are two different physical pictures. One suggests that the AFM order is a spin density wave (SDW) which is driven by Fermi surface nesting between the electron pockets at M point and hole pockets at Γ point based on band structural calculations^{12,16}. The other suggests that the AFM order stems from the short range magnetic exchange coupling between local moments^{17,18,19,20}. However, regardless of the origin of

the AFM ordering, the theories suggest that the superconductivity is tied to the magnetism in the FeAs-based materials^{16,17,20,21}. The investigation on the structural properties and AFM ordering of the parent compounds can shed light on the mechanism of high- T_c superconductivity.

The structural and magnetic transitions in the FeAs-based parent compounds are deeply connected. For the first discovered 1111 type systems, neutron scattering studies on the $R\text{FeAsO}$ ($R = \text{La, Ce, Nd, and Sm}$) samples have found that the structural phase transition occurs first as temperature decreases, and then magnetic ordering associated with Fe ions follows^{13,22}, in contrast to the case in 122-type systems where both structural transition and AFM order occur at the same temperature¹⁴. Recent report on isotope effect also shows positive isotope effect on both T_c and AFM ordering temperature²³. Some theoretic studies proposed that the structural transition is directly driven by the AFM order^{17,19,24}. In particular, a theory based on a Heisenberg-type local moment exchange model suggests that the structural transition can be driven by a nematic Ising magnetic order due to the presence of intrinsic magnetic frustration¹⁹. The theory¹⁹ predicts that the difference between the structural and magnetic transition temperatures is controlled by the magnetic coupling between layers: the difference becomes larger when the coupling is weakened. Recent neutron experiment results in 4% Ni-doped BaFe_2As_2 have supported this prediction²⁵.

In this paper, we report the investigation of structural phase transition detected by means of low-temperature X-ray diffraction (XRD) in the parent compounds LaFeAsO , SmFeAsO , GdFeAsO , and TbFeAsO . The AFM order temperatures associated with Fe ions (T_{N1}) and the AFM ordering temperatures (T_{N2}) associated with the magnetic rare earths Sm, Gd and Tb are also obtained by measuring magnetic susceptibility and trans-

*Electronic address: zhuan@zju.edu.cn

port properties. A systematic comparison of the structural transition temperature (T_S) with T_{N1} is made. As R is changed from La, through Sm and Gd, to Tb, both the c -axis and a -axis lattice constants decrease significantly. Meanwhile both T_S and T_{N1} decrease monotonously. It is also found that the temperature gap ($T_S - T_{N1}$) becomes smaller when the distance between FeAs layers becomes shorter. Therefore, our experimental results provide concrete evidence supporting the theory proposed in Ref.¹⁹ and suggest the dimensionality may have important effect on the AFM ordering and on the superconductivity mechanism as well.

II. EXPERIMENTAL

The polycrystalline $R\text{FeAsO}$ ($R = \text{La, Sm, Gd, Tb}$) samples were synthesized by solid state reaction in vacuum using powders of $R\text{As}$, $R_2\text{O}_3$ (for TbFeAsO , Tb_4O_7 was used instead), FeAs and Fe_2As . $R\text{As}$ was presynthesized by reacting stoichiometric R pieces and As powders in evacuated quartz tubes at 1223 K for 24 hours. FeAs and Fe_2As were prepared by reacting stoichiometric Fe powders and As powders at 1023 K for 20 hours. The powders of these intermediate materials were weighed according to the stoichiometric ratio of $R\text{FeAsO}$ respectively, and then thoroughly mixed in an agate mortar. The mixtures were pressed into pellets under a pressure of 4000 kg/cm². All the processes were operated in a glove box filled with high-purity argon. The pellets were sealed in evacuated quartz tubes and heated uniformly at 1433-1453 K for 40 hours.

The sample purity was first checked by measurements of powder X-ray diffraction (XRD) at room temperature using a D/Max-rA diffractometer with $\text{Cu K}\alpha$ radiation and a graphite monochromator. Low temperature X-ray diffraction (LTXRD) measurements for powder specimens were performed using the RINT 2500 system, Rigaku Co. An X-ray beam was generated by a rotating Cu anode. The specimens were cooled by a ^4He gas circulating cryo-cooler and can be cooled down to about 10 K. The temperature stability is better than 0.1% during the LTXRD measurements. At several temperatures entire profiles of reflection peaks were measured with a step size of 0.01° and a step-counting time of 6 s and refined by the Rietveld method using the reported crystal structure. For some reflection planes X-ray diffraction measurements with a step size of 0.005° and a step-counting time of 60 s were performed to accumulate more counts at certain temperatures. From the observed profile the d value of (220) peak, the integrated intensity ($I.I.$) and also the full-width-at-half-maximum ($FWHM$) were obtained. In these analysis the profile was fitted to a Pseudo-Voigt function.

The electrical resistivity was measured by a standard four-terminal method. The samples for transport property measurements were cut into a thin bar. The temperature dependence of d.c. magnetic susceptibility was

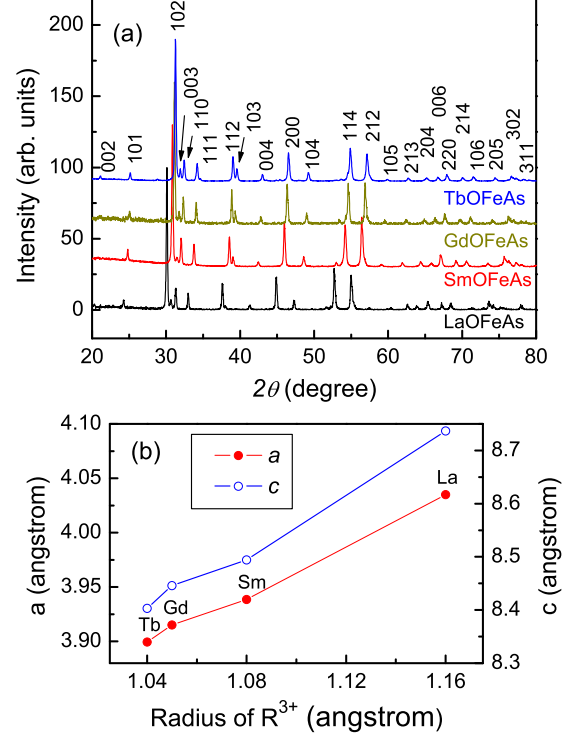


FIG. 1: (Color online) (a) X-ray powder diffraction pattern at room temperature of $R\text{FeAsO}$ ($R = \text{La, Sm, Gd, Tb}$); (b) the variations of lattice constants a and c with the radius of R ions. The radius of R ions is taken from Ref.²⁶.

measured on a Quantum Design magnetic property measurement system (MPMS-5) under magnetic field of 1000 Oe.

III. RESULTS AND DISCUSSION

Fig. 1(a) shows the room-temperature XRD patterns of $R\text{FeAsO}$ ($R = \text{La, Sm, Gd, Tb}$) samples and Fig.1(b) shows the variations of lattice constants a and c with the radius of R ions. For all the four parent compounds, the XRD peaks can be well indexed based on a tetragonal cell with the space group of $P4/nmm$ (No. 129), which indicates that the samples are in a uniform single phase without obvious trace of impurity phases. As R is changed from La to Sm, Gd, and then Tb, all the peaks shift to larger 2θ 's significantly, implying a remarkable shrinkage of lattice in both a -axis and c -axis directions. This result is consistent with the fact that the radius of R ions decreases gradually as R goes from the light to heavy rare earth elements²⁶. It can also be found from Fig.1(b) that the c -axis shrinks slightly more quickly than the a axis does.

Fig. 2 shows the temperature dependence of resistiv-

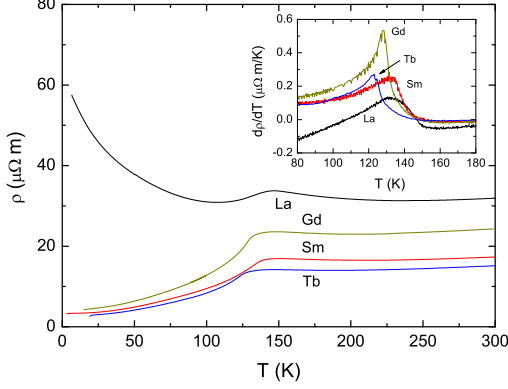


FIG. 2: (Color online) Temperature dependent resistivity of $RFeAsO$ ($R = La, Sm, Gd, Tb$). Inset: the derivative of resistivity ($d\rho/dT$) as a function of temperature.

ity for the $RFeAsO$ samples. The resistivity starts to drop around 120-150 K. To show the drop position more precisely, we calculated the derivative $d\rho/dT$ versus T as shown in the inset of Fig.2. The resistivity for $LaFeAsO$ shows an upturn at low temperatures, but it remains metallic for $RFeAsO$ with $R = Sm, Gd$, and Tb . Similar resistivity has been observed in other 1111-type parent compounds with magnetic rare earth elements²⁷. Such a difference in low temperature resistivity has not been well understood yet. We define the characterization temperature T_{N1} as the peak position in the curves of $d\rho/dT$ versus T . As shown in the inset, T_{N1} decreases significantly as R is changed from La to Sm, Gd , and Tb . Neutron studies have confirmed that the resistivity anomaly is caused by the structural phase transition and the following formation of antiferromagnetic SDW state¹³. Previous reports have proposed that the peak position in $d\rho/dT$ corresponds to the AFM ordering of Fe ions moments rather than the structural phase transition^{27,28}. Indeed, the studies of neutron diffraction reported that the AFM ordering temperature of $LaFeAsO$ is about 135 K, about 20 K lower than the structural phase transition temperature T_S of 158 K¹³. The T_{N1} value of $LaOFeAs$ determined from the resistivity is 132 K, consistent with the AFM order temperature reported by the neutron diffraction. The AFM order temperature determined from the measurements of Mössbauer spectroscopy and μSR relaxation is also in agreement with T_{N1} , the peak temperature in the $d\rho/dT$ versus T curves²⁸. Thus we can regard T_{N1} as the characteristic temperature at which the magnetic moments of Fe ions become AFM ordered. For $R = Sm, Gd$, and Tb , T_{N1} is 133 K, 128 K, and 122 K, respectively.

In order to obtain more information about the magnetism associated with Fe ions and R^{3+} ions as R is magnetic rare earth elements other than La , the magnetic susceptibility of $RFeAsO$ ($R = Sm, Gd, Tb$) was measured

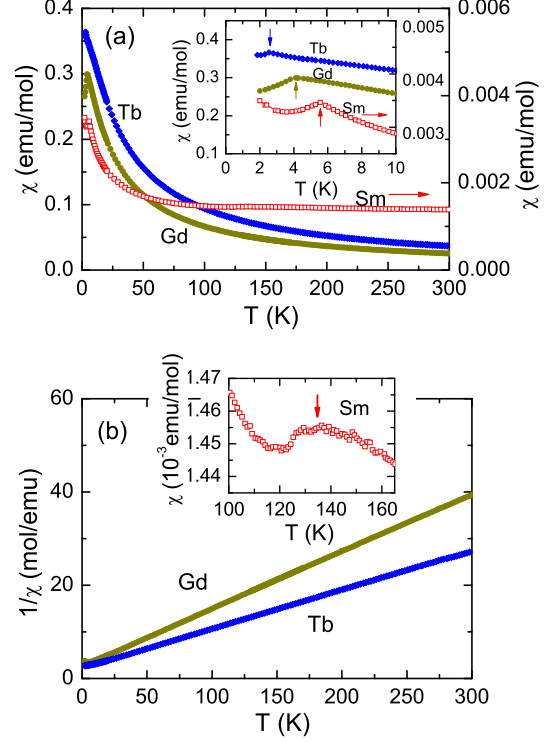


FIG. 3: (Color online) (a) Temperature dependence of magnetic susceptibility measured under H of 1000 Oe for $SmFeAsO$, $GdFeAsO$ and $TbFeAsO$. Inset: enlarged plot for low temperatures to show the AFM transitions of R^{3+} ions; (b) The plot of χ^{-1} versus T for $GdFeAsO$ and $TbFeAsO$. The linear behavior for $T > T_{N2}$ means that χ can be fitted by the Curie-Weiss law very well. Inset: Enlarged plot for $SmFeAsO$ to show the kink around the AFM ordering temperature (T_{N1}) of Fe ions.

under the magnetic field of 1000 Oe, as shown in Fig.3. From the temperature dependence of magnetic susceptibility shown in Fig. 3(a) and its inset, it can be found that the $GdFeAsO$ and $TbFeAsO$ have much larger magnetic susceptibility compared to $SmFeAsO$ because Gd^{3+} and Tb^{3+} ions have much larger magnetic moments. At low temperatures, clear phase transitions caused by the AFM ordering of the magnetic moments of R ions can be found at T_{N2} . The AFM order temperature of R ions, i.e., T_{N2} determined in our measurements, is 5.56 K, 4.11 K, and 2.54 K for $SmFeAsO$, $GdFeAsO$, and $TbFeAsO$, respectively, consistent with previous reports^{7,29,30}. For $SmFeAsO$, as shown in the inset of Fig.3(b), a kink associated with the AFM ordering of Fe ions can be observed around 134 K, consistent with the T_{N1} value of 133 K within the experimental error. For $GdFeAsO$ and $TbFeAsO$, this kind of AFM order associated with Fe ions is buried in the large magnetic signals from the R^{3+} ions. The magnetic contributions from the R^{3+} ions obey the Curie-Weiss law very well. As shown in the Fig.3(b), the

inverse of χ increases strictly linearly with T as $T > T_{N2}$. For the SmFeAsO sample, the magnetic susceptibility does not exhibit the Cuire-Weiss behavior because the contribution from the Fe ions which is linearly dependent on temperature is comparable to the contribution from the Sm^{3+} ions³¹. By fitting the Curie-Weiss law, we obtained that the effective magnetic moments p_{eff} are 8.0, and 9.7 $\mu_B/f.u.$ for GdFeAsO and TbFeAsO respectively, which are consistent with the theoretical values of magnetic moments of free Gd^{3+} and Tb^{3+} ions. If we subtract the Curie-Weiss term which should originate from the contributions of R^{3+} ions, we can also find a slight drop in the subtracted term ($\chi - \chi_{CW}$) around T of 120-140 K for GdFeAsO and TbFeAsO (not shown here), where χ_{CW} is the Cuire-Weiss fitting function. But it is very hard to distinguish whether such a drop in $\chi - \chi_{CW}$ occurs at the AFM order temperature of Fe ions or the structural phase transition temperature. Therefore, we will take T_{N1} as the transition temperature associated with the AFM order of Fe ions.

As mentioned above, the neutron studies¹³ have revealed that a structural phase transition occurs just before the AFM ordering in LaFeAsO. It is generally believed that the structure of the parent compounds $R\text{FeAsO}$ transforms from tetragonal to orthorhombic when the temperature is lower than the structural transition temperature T_S . Such a structure phase transition can be detected by the splitting of (220) peak in the low temperature x-ray diffraction. Fig. 4 shows the temperature dependence of the (220) peak d value for $R\text{FeAsO}$ samples. The inset shows the intensity of (220) peak before (blue lines) and after (red lines) structure phase transition. It can be seen that the (220) peak splits into two peaks when the temperature is lower than the structural phase transition temperature. From the temperature dependence of (220) peak d -value, the structural phase transition temperature T_S can be easily determined as the splitting point of this peak. As R changes from La to Tb, the (220) peak d value decreases significantly, and T_S decreases as well.

We summarize the variations of the structural phase transition temperature (T_S) and AFM ordering temperature (T_{N1}) in Fig. 5. The structural and physical parameters for these four parent compounds are also listed in Table I. As R is changed from La, through Sm and Gd, to Tb, not only T_S and T_{N1} decrease significantly, but the temperature gap between T_S and T_{N1} also becomes smaller, i.e., the AFM transition occurs at the temperature closer to the structural phase transition temperature. Actually the structural phase transition and AFM ordering happen simultaneously in the more three-dimensional 122 parent compounds like BaFe_2As_2 .

The experimental results can be understood within the theory proposed in Ref.¹⁹ where an effective Heisenberg-type magnetic exchange model, the so called J_1 - J_2 - J_z model with J_1 , J_2 and J_z being the in-plane nearest neighbor (NN), in-plane next nearest neighbor (NNN) and out-of-plane magnetic exchange couplings respectively, explains both the structural and magnetic transitions as-

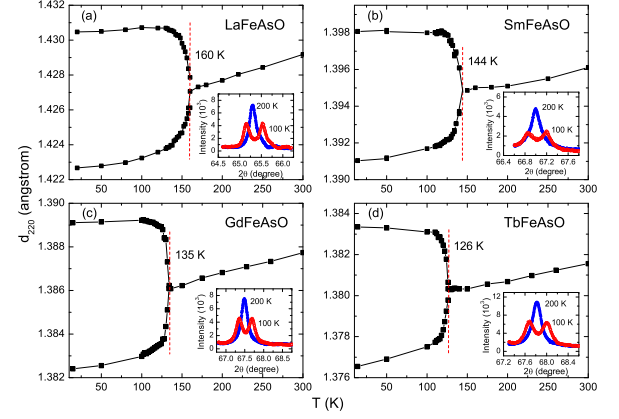


FIG. 4: (Color online) The temperature dependence of the (220) peak d value for LaFeAsO (a), SmFeAsO (b), GdFeAsO (c) and TbFeAsO (d). The insets show the intensity of (220) peak before (blue lines) and after (red lines) structure phase transition.

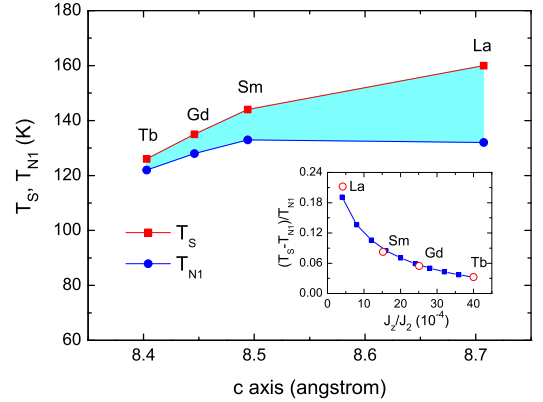


FIG. 5: (Color online) Plot of structural phase transition temperature T_S , and magnetic transition temperature T_{N1} associated to the AFM order of Fe ions, versus the c -axis for $R\text{FeAsO}$ ($R = \text{La, Sm, Gd, Tb}$). Inset: plot of $(T_S - T_{N1})/T_{N1}$ versus J_z/J_2 . The open circles denote the experimental data of $(T_S - T_{N1})/T_{N1}$, and the solid squares denote the theoretical values. See text for details.

sociated with the FeAs layers. In this model, a collinear AFM ground state is obtained when J_1 is less than $2J_2$, and a nematic Ising magnetic order transition that breaks lattice rotational symmetry takes place at a temperature equal to or higher than the collinear AFM transition temperature¹⁹. By including the lattice and spin coupling, the nematic order naturally produces an orthorhombic lattice distortion. Therefore, the model captures both structural and magnetic transitions and suggests the structural transition be driven magnetically. A

TABLE I: Structural and Physical parameters of $R\text{FeAsO}$ ($R = \text{La, Sm, Gd, and Tb}$)

Sample	$r(R^{3+})$ (Å)	a (Å)	c (Å)	T_S (K)	T_{N1} (K)	T_{N2} (K)
LaFeAsO	1.16	4.0349	8.7366	160	132	-
SmFeAsO	1.08	3.9385	8.4941	144	133	5.56
GdFeAsO	1.05	3.9151	8.4660	135	128	4.11
TbFeAsO	1.04	3.8994	8.4029	126	122	2.54

quantitative prediction of this model is that the difference between the structural and AFM transition temperature is determined by the ratio between J_z and J_2 , i.e., J_z/J_2 . The AFM transition temperature, $T_{N1} \propto J_2/\log(J_2/J_z)$. Using the calculated results in Ref.¹⁹ and assuming that $J_1 \approx J_2$, we find that the ratio J_z/J_2 for the four typical parent compounds (La, Sm, Gd, Tb)FeAsO are (4.10, 15.2, 25.1, 40.0) $\times 10^{-4}$. The out-of-plane magnetic exchange coupling increases quickly as the lattice constant along c -axis decreases, and therefore the temperature difference between T_S and T_{N1} should decrease according to this model. The result is plotted in the inset of Fig.5. The experimental data of $(T_S - T_{N1})/T_{N1}$ are in agreement with the theoretical calculations. By measuring the spin wave gap around the wavevector $(0, \pi, 0)$ as shown in Ref.³² in future neutron scattering experiments, the value of J_z can also be independently obtained.

IV. CONCLUSION

In summary, we have studied the structural phase transition of four parent compounds $R\text{FeAsO}$ ($R=\text{La, Sm, Gd, Tb}$) by measuring low-temperature X-ray diffractions. As R is changed from La to Tb, T_s and T_{an} as well as the c axis decrease significantly. Furthermore, the temperature difference between T_S and T_{N1} becomes smaller as the c axis becomes shorter. According to the theoretical calculations proposed in Ref.¹⁹, the out-of-plane magnetic exchange coupling increases quickly with the decreasing c -axis lattice constant and therefore the temperature difference between T_S and T_{N1} is significantly influenced. The experimental data of $(T_S - T_{N1})/T_{N1}$ are in agreement with the theoretical calculations. This result supports the theoretical proposal that the structural phase transition is driven by a nematic Ising magnetic order due to the presence of intrinsic magnetic frustration, and indicates that the dimensionality could have important effect on the AFM ordering, and the magnetism may play an important role in high- T_c superconductivity of the iron pnictides.

Acknowledgments

This work is supported by the National Science Foundation of China (No. 10634030), PCSIRT (No. IRT0754), and the National Basic Research Program of China (No.2006CB601003 and 2007CB925001).

-
- ¹ Y. Kamihara, H. Hiramatsu, M. Hirano, R. Kawamura, H. Yanagi, T. Kamiya, and H. Hosono, *J. Am. Chem. Soc.* **128**, 10012 (2006).
 - ² Y. Kamihara, T. Watanabe, M. Hirano, and H. Hosono, *J. Am. Chem. Soc.* **130**, 3296 (2008)
 - ³ X. H. Chen, T. Wu, G. Wu, R. H. Liu, H. Chen, and D. F. Fang, *Nature*. **453**, 761 (2008)
 - ⁴ G. F. Chen, Z. Li, D. Wu, G. Li, W. Z. Hu, J. Dong, P. Zheng, J. L. Luo, and N. L. Wang, *Phys. Rev. Lett.* **100**, 247002 (2008)
 - ⁵ Z. Ren, G. Che, X. Dong, J. Yang, W. Lu, W. Yi, X. Shen, Z. Li, L. Sun, F. Zhou, and Z. Zhao, *Europhys. Lett.* **83**, 17002 (2008)
 - ⁶ H. H. Wen, G. Mu, L. Fang, H. Yang, and X. Zhu, *Europhys. Lett.* **82**, 17009 (2008)
 - ⁷ C. Wang, L. Li, S. Chi, Z. Zhu, Z. Ren, Y. Li, Y. Wang, X. Lin, Y. Luo, X. Xu, G. Cao, and Z. Xu, *Europhys. Lett.* **83**, 67006 (2008)
 - ⁸ Z. Li, G. Chen, J. Dong, G. Li, W. Hu, D. Wu, S. Su, P. Zheng, T. Xiang, N. Wang, and J. Luo, *Phys. Rev. B* **78**, 060504(R) 2008
 - ⁹ M. Rotter, M. Tegel, and D. Johrendt, *Phys. Rev. Lett.* **101**, 107006 (2008)
 - ¹⁰ X. C. Wang, Q. Q. Liu, Y. X. Lv, W. B. Gao, L. X. Yang, R. C. Yu, F. Y. Li, C. Q. Jin, *Solid State Commun.* **148**, 538 (2008)
 - ¹¹ F. C. Hsu, J. Y. Luo, K. W. Yeh, T. K. Chen, T. W. Huang, P. M. Wu, Y. C. Lee, Y. L. Huang, Y. Y. Chu, D. C. Yan, and M.-K. Wu, arXiv: 0807.2369 (2008)
 - ¹² J. Dong, H. J. Zhang, G. Xu, Z. Li, G. Li, W. Z. Hu, D. Wu, G. F. Chen, X. Dai, J. L. Luo, Z. Fang, and N. L. Wang, *Europhys. Lett.* **83**, 27006 (2008)
 - ¹³ C. de la Cruz, Q. Huang, J. W. Lynn, J. Y. Li, I. W. Ratcliff, J. L. Zarestky, H. A. Mook, G. F. Chen, J. L. Luo, N. L. Wang, and P. C. Dai, *Nature* **453**, 899 (2008)
 - ¹⁴ Q. Huang, Y. Qiu, W. Bao, M. A. Green, J. W. Lynn, Y. C. Gasparovic, T. Wu, G. Wu, and X. H. Chen, *Phys. Rev. Lett.* **101**, 257003 (2008)
 - ¹⁵ T. Watanabe, H. Yanagi, Y. Kamihara, T. Kamiya, M. Hirano, and H. Hosono, arXiv:0805.4340 (2008)
 - ¹⁶ I. I. Mazin, D. J. Singh, M. D. Johannes, and M. H. Du, *Phys. Rev. Lett.* **101**, 057003 (2008)
 - ¹⁷ T. Yildirim, *Phys. Rev. Lett.* **101**, 057010 (2008)
 - ¹⁸ Q. M. Si and E. Abrahams, *Phys. Rev. Lett.* **101**, 076401 (2008)
 - ¹⁹ C. Fang, H. Yao, W. F. Tsai, J. P. Hu, and S. A. Kivelson, *Phys. Rev. B* **77**, 224509 (2008)
 - ²⁰ F. Ma, Z. -Y. Lu, and T. Xiang, *Phys. Rev. B* **78**, 224517 (2008)
 - ²¹ K. Seo, B. A. Bernevig, and J. P. Hu, *Phys. Rev. Lett.* **101**, 206404 (2008)
 - ²² J. W. Lynn and P. Dai, *Physica C* **469**, 469 (2009)
 - ²³ R. H. Liu, T. Wu, G. Wu, H. Chen, X. F. Wang, Y. L. Xie, J. J. Yin, Y. J. Yan, Q. J. Li, B. C. Shi, W. S. Chu, Z. Y. Wu, and X. H. Chen, *Nature* **459**, 64 (2009)
 - ²⁴ C. Xu, M. Müller and S. Sachdev, *Phys. Rev. B* **78**,

- 020501(R) (2008)
- ²⁵ L. W. Harriger, A. Schneidewind, S. Li, J. Zhao, Z. Li, W. Lu, X. Dong, F. Zhou, Z. Zhao, J. Hu, and P. Dai, arXiv: 0904.3775 (2009)
- ²⁶ R. D. Shannon, *Acta. Crystallogr. A* **32**, 751 (1976)
- ²⁷ M. A. McGuire, R. P. Hermann, A. S. Sefat, B. C. Sales, R. Jin, D. Mandrus, F. Grandjean, and G. J. Long, *New J. Phys.* **11**, 025011 (2009)
- ²⁸ H.-H. Klauss, H. Luetkens, R. Klingeler, C. Hess, F. J. Litterst, M. Kraken, M. M. Korshunov, I. Eremin, S.-L. Drechsler, R. Khasanov, A. Amato, J. Hamann-Borrero, N. Leps, A. Kondrat, G. Behr, J. Werner, and B. Büchner, *Phys. Rev. Lett.* **101**, 077005 (2008)
- ²⁹ L. Ding, C. He, J. K. Dong, T. Wu, R. H. Liu, X. H. Chen, and S. Y. Li, *Phys. Rev. B* **77**, 180510(R) (2008)
- ³⁰ L. J. Li, Y. K. Li, Z. Ren, Y. K. Luo, X. Lin, M. He, Q. Tao, Z. W. Zhu, G. H. Cao, and Z. A. Xu, *Phys. Rev. B* **78**, 132506 (2008)
- ³¹ G. M. Zhang, Y. H. Su, Z. Y. Lu, Z. Y. Weng, D. H. Lee, and T. Xiang, *Europhys. Lett.* **86**, 37006 (2009)
- ³² J. Zhao, D. T. Adroja, D.-X. Yao, R. Bewley, S. Li, X. F. Wang, G. Wu, X. H. Chen, J. Hu, and P. Dai, *Nature Phys.* **5**, 555 (2009)